# Comprehensive Circuit Model of Autolimiting Superconductor Devices

J. Mateu, *Senior Member, IEEE*, C. Collado, *Senior Member, IEEE*, A. Hueltes, J. M. O'Callaghan, *Senior Member, IEEE*, D. Garcia-Pastor, R. Perea-Robles, N. Joshi, X. Lu, N. Orloff, and J. C. Booth

***Abstract*—This paper presents a phenomenological equivalent circuit to model the phenomenon occurring when a section of superconducting transmission line transits from a superconducting state to a normal state. This phenomenon allows the use of superconductors for the design of autolimiting structures based on superconducting transmission line sections. Although this autolimiting effect happens when the current density achieved in the superconductor exceeds the critical current inherent to the superconducting material, heating effects also play a significant role in this behavior. The equivalent circuit presented in this work accounts for both electric and thermal effects, and the interaction between them. The circuit model is then used for the evaluation of a practical microwave and frequency selective IMUX configuration.**

***Index Terms*—Nonlinearity, heating effects, autolimiting, microwave devices, filters.**

## I. Introduction

THE use of superconducting (HTS) auto-limiting structures has been proven over the past few years through the realization of power-limiting superconductor transmission lines [1]–[2], which exploit the transition phenomenon from superconductor to normal state. This achievement suggests the use of superconductors on the design of complex, frequency-selective, and functional auto-limiting architectures [3]. Application of those devices are several, including radar protection from jamming signals and the coexistence between very different RF/microwave systems, such as cellular communication and high-power radars. When these systems coexist, they need to operate without mutual interference or hardware damage. This challenge motivates continued research on novel multifunctional devices.

In response to this challenge, our work presents a phenomenological circuit model that accounts for the transition of the HTS section from the superconducting state to the normal state. This transition is responsible for the auto-limiting function.

Manuscript received August 31, 2016; accepted December 6, 2016. Date of publication December 12, 2016; date of current version January 6, 2017. This work was supported in part by the Generalitat de Catalunya under Grant 2014 SGR 1551 and in part by the U.S. Government.

J. Mateu, C. Collado, A. Hueltes, J. M. O'Callaghan, D. Garcia-Pastor, and R. Perea-Robles are with the Department of Signal Theory and Communication, Universitat Politecnica de Catalunya, Barcelona 08034, Spain (e-mail: jmateu@tsc.upc.edu).

N. Joshi, X. Lu, N. Orloff, and J. C. Booth are with the CTL, National Institute of Standards and Technology, Boulder, CO 80305 USA.

Color versions of one or more of the figures in this paper are available online at http://ieeexplore.ieee.org.

Digital Object Identifier 10.1109/TASC.2016.2638419

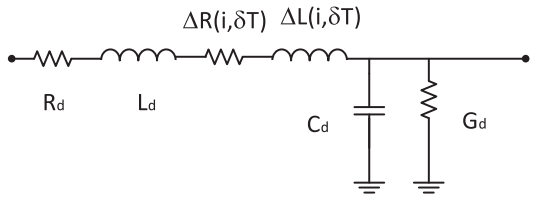


Fig. 1. Elemental section *dz* of a superconducting transmission line that includes non-linear intrinsic and heating effects [4].

The circuit model may be used to evaluate the auto-limiting performance of a complex structure such as a frequency selective multiplexer. In this work, a conventional circulator-coupled multiplexer is assessed under several realistic scenarios. These scenarios address the limiting effects in both the channel where the jamming signal occurs and in adjacent channels. This analysis may be used to verify the suitability of the multiplexer configuration.

Note that this work goes one step beyond previous work [3] and [4]. In [3], we evaluated the limiting effect of a single channelizing filter without considering thermal effects, whereas in [4], we proposed a local electro-thermal model that was only used to evaluate the limiting effects of superconducting transmission lines. This work complements both by developing a new phenomenological electro-thermal model, and by evaluating the limiting effects in a practical multiplexing configuration.

## II. Electro-Thermal Model in a Superconducting Transmission Line Section

Superconductors have the ability to switch from a high-loss normal state to a low-loss superconducting state, when cooled down to the critical temperature $T_c$. This transition also occurs for high-power signals when the current density in the superconductor exceeds the critical current $j_c$, due to the non-linear surface impedance [5]. For a quasi-TEM propagation mode, as occurs in a section of transmission line, an equivalent circuit model as the one shown in Fig. 1 can be outlined [5]. This circuit model corresponds to an elemental section *dz* where $L_d$, $R_d$, $C_d$ and $G_d$, correspond to the inductance, resistance, capacitance and conductance, per unit length, at the operating temperature. The additional terms $\Delta L(i, \delta T)$ and $\Delta R(i, \delta T)$ represent the distributed nonlinear inductance and resistance, respectively. These account for the superconducting transition, and depend on the current, $i$, flowing through the line and the temperature rise in the superconductor $\delta T$.

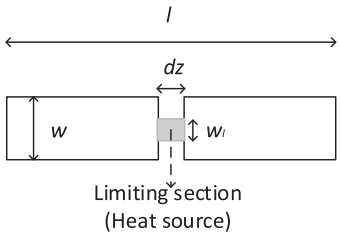


Fig. 2. Superconducting transmission line with an inserted SLS, *dz*.

Determination of these linear and non-linear terms is crucial for creating an accurate circuit model of superconducting devices. The distributed inductance and resistance are obtained by means of the method described in [5]–[7]. These methods calculate the current density distribution along the cross-section of the limiting transmission line. Application of the current distribution through the non-linear conductivity is then used to obtain the distributed terms $L_d$ and $R_d$, and its corresponding non-linear terms $\Delta L(i,0)$ and $\Delta R(i,0)$.

At low powers, the temperature rise due to self-heating is negligible ($\delta T = 0$) because the losses are very small. But at higher powers, the losses start to increase and the dissipation increases. This then produces a temperature rise ($\delta T > 0$), which contributes to the transition to normal state, and therefore to the limiting effect [4].

In order to account for the temperature rise effect, we apply the methodology developed in our previous work [4], where a local thermal model was used along with the non-linear current dependence, to obtain $\Delta L(i, \delta T)$ and $\Delta R(i, \delta T)$.

Complete modeling of the electro-thermal phenomena that occurs in the limiting effect requires consideration of not only the electromagnetic terms of the dielectric $C_d$ and $G_d$, which can be obtained from several EM simulators, but also requires consideration of the heat conduction through the dielectric. A thermal model of the dielectric and its coupling into the electromagnetic and self-heating effects in the circuit of Fig. 1 are detailed in the following section.

## III. Thermal Effect of the Substrate

This section outlines the procedure to model the heating flow through the dielectric supporting the superconducting limiting section (SLS). As in [3] the SLS consists of a small segment of superconducting transmission line $d_z$ with much narrower strip section $w_l$, as outlined in Fig. 2.

When the SLS is in its normal-metal state, it dissipates power and acts as a heating source. In turn, this heat is spread throughout the dielectric. The distribution of heat through the dielectric can be modeled as a thermal resistance, which connects the heating source (SLS) through the convection boundary conditions [8].

The total thermal resistance is defined by $R_T = (\overline{T_s} - T_{\rm phys})/Q$, where $\overline{T_s}$ is the average temperature in the heating source, $T_{\rm phys}$ is the temperature of the cold plate set at the operating temperature and $Q$ is the heat flow rate, which can be calculated from circuit analysis.

Under this assumption, an analytical solution can be used to solve for an eccentric heat source on a finite rectangular flux channel in an isotropic substrate [8]. Details of the heating scenario are given in Fig. 3. Fig. 3a shows the top view of the

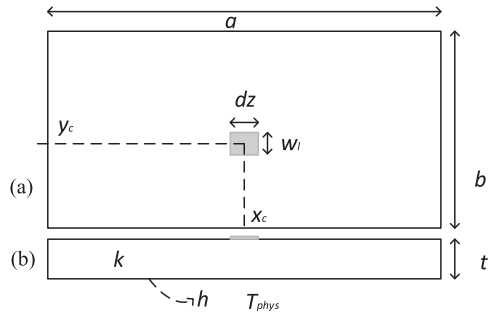


Fig. 3. Heating source on top of the substrate. (a) Top view, (b) side view.

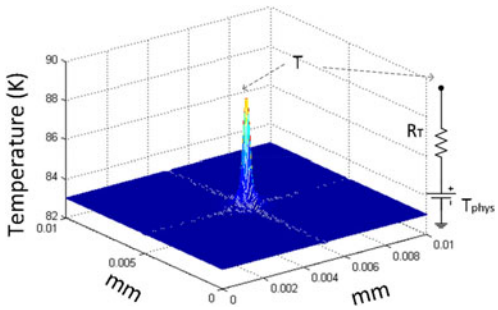


Fig. 4. Temperature distribution along the top surface of the substrate. Right side inset: Thermal modeling of the temperature rise.

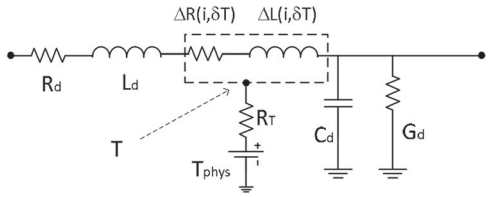


Fig. 5. Elemental section *dz*, of a SLS, considering the non-linear intrinsic effects and heating effect. Additionally, the heating flow through the substrate is included.

aforementioned heating source on the dielectric. Dimensions ($d_z$ and $w_l$) and position ($x_c$ and $y_c$) of the heating source correspond to the area of the SLS and its location on the substrate. Fig. 3b shows the side view of the heating source, where *t* is the substrate thickness, *k* is the thermal conductivity of the substrate and *h* is the heat transfer coefficient.

To illustrate this, Fig. 4 shows the temperature on top of the dielectric when a heating source is placed in the middle of the dielectric. The heating source consists of a SLS placed on top of a sapphire substrate, where $w_l = 10\,\mu$m, $d_z = 0.2\,$mm ($\approx \lambda/15$), $a = b = 10\,$mm, $t = 0.5\,$mm, $k = 42\,\mathrm{W/(K \cdot m)}$, and a heat flow rate of $Q = 0.1\,$W is assumed. The substrate is thermally connected to the chuck operating at $T_{\rm phys} = 83\,$K. The temperature rise observed in Fig. 4 can be model by the thermal resistance, as indicated in the right side of Fig. 4, where $R_T = 63\,\Omega$. Identical simulation for a quartz substrate with $k = 2\,\mathrm{W/(K \cdot m)}$, results in a higher thermal resistance $R_T = 1300\,\Omega$. These two values will be used in Section IV.

The thermal model outlined in the inset of Fig. 4 can be coupled to the electromagnetic domain, as indicated in Fig. 5.

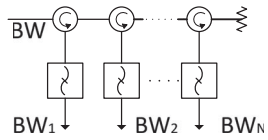


Fig. 6. Multiplexing architecture based on a Circulator-Coupled approach.

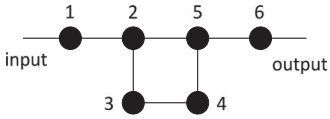


Fig. 7. Single limiting channel of the hybrid-coupled approach, under the limiting concept of [10].

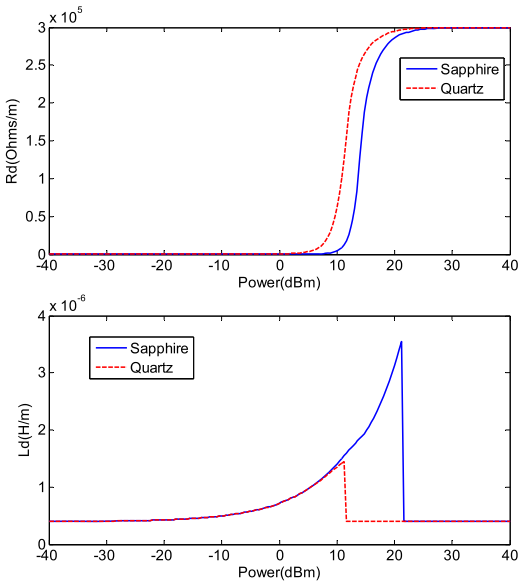


Fig. 8. Distributed resistance and inductance as a function of power.

As indicated above. $T_{\rm phys}$ is the reference temperature set by the boundary conditions at the bottom of the substrate, where the sample is usually in very good thermal contact with a copper chuck to keep the sample thermally stable at the desired operating temperature. The dissipated power (heat) is used as the input for the thermal domain model and the temperature rise is obtained at the SLS, defining the value of the distributed inductance and resistance at a given power.

## IV. Autolimiting Superconducting Multiplexer

The circuit model described above is used to evaluate the performance of a frequency-selective, auto-limiting superconducting multiplexing candidate. The configuration of the multiplexing approach is based on a conventional architecture, see Fig. 6 [9]. This approach uses circulators to route the full bandwidth (BW) signal to each channelizing filter, $\mathrm{BW_i}$. Only two channels are considered in this work, where the channelizing filters $\mathrm{BW_1}$ and $\mathrm{BW_2}$ have an identical bandwidth of 80 MHz, being centered at 3.5 GHz and 3.7 GHz, respectively. All filters consist of a sixth order Chebyshev response with a single pair of transmission zeros, symmetrically placed at the normalized frequency of $+/-j\cdot 1.75$. Evaluation of the filters assume a topology based on halfwave 50 Ω superconducting-transmission-line coupled

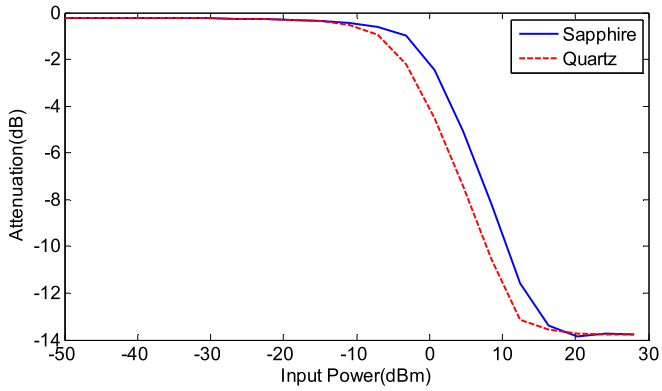


Fig. 9. In-band attenuation as a function of the input power.

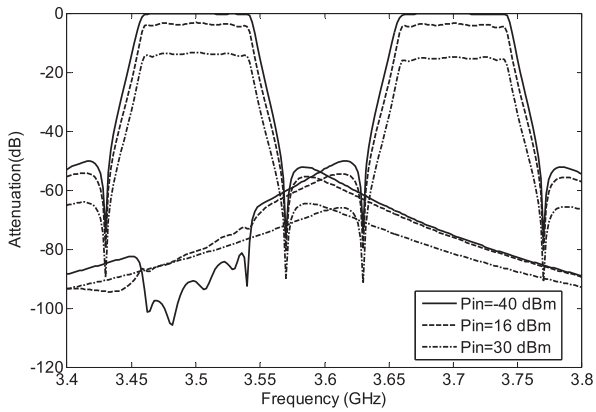


Fig. 10. Attenuation frequency dependence. Note that this corresponds to the transmission $S_{21}$ term for each input power, Pin.

resonators [9]. The filter topology is outlined in Fig. 7, where each resonator is indicated by a black circle and the lines indicate the coupling between resonators. Creation of transmission zeros has been performed by cross coupling between resonators 2 and 5 [9].

### A. Limiting Section

To evaluate the limiting performance, a SLS such as the one shown in Fig. 2 will be inserted in the middle of one of the six resonators that form the filter. Note that in a λ/2 resonant transmission line, the maximum current occurs in the middle of the resonator.

The dimensions of the SLS, properties of the substrates and operating temperature are the same at those listed in Section III. The additional properties of the SLS that are used in this section are 150 $\mu$m of thickness, $T_c = 90$ K and $j_c = 5\times 10^{10}$ A/m$^2$. Analysis for both substrates (sapphire and quartz) is also considered in the analysis. Values of the distributed resistance and inductance of the phenomenological model of Fig. 4, as a function of power, are shown in Fig. 8. These dependencies are consistent with the ones reported in [4], for the local approach.

### B. Simulation Scenarios

In order to assess the suitability of this multiplexing configuration, several scenarios have been considered: The first scenario evaluates the effects in a single channelizing filter. This would assume an isolated filter with a high-power jamming

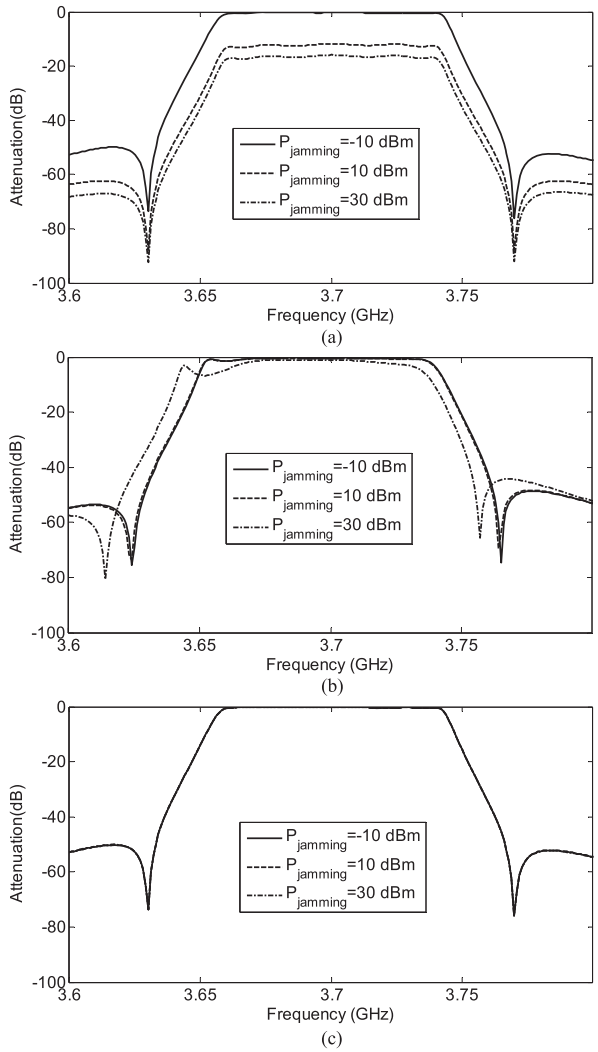


Fig. 11. Filter attenuation response ($S_{21}$ parameter) when a jamming signal of $-10$ dBm, 10 dBm and 30 dBm is set at the adjacent channel. (a) SLS at the first resonator, (b) SLS at the 3rd resonator and (c) SLS at the last resonator.

signal at the central frequency of the filter (3.5 GHz for filter $BW_1$). The SLS is placed in the middle of resonator 1. Fig. 9 shows the attenuated signal as a function of the input power. The solid line corresponds to dielectric sapphire, whereas the dashed line corresponds to quartz. As expected, there is less attenuation for sapphire, until complete saturation is achieved. The second scenario outlines the frequency dependence of the attenuation when a high-power signal is swept over the multiplexer bandwidth. This case only considers the sapphire substrate and, as in previous case, the SLS is placed in resonator 1. Results are shown in Fig. 10, for input powers of $-40$, 16 and 30 dBm. Note that the filter performance is barely affected and only an increase of insertion losses is observed over the whole bandwidth. This is because the current in the first resonator is barely modified along the band, so the limiting effect is almost equal. The third scenario looks at the effect of a jamming signal in an adjacent channel. In particular, a jamming signal is set at the central frequency of the first filter at 3.5 GHz and the performance of the second filter from 3.6 to 3.8 GHz is observed. Under this scenario, we consider three different cases: the SLS is set in resonator 1 (Fig. 11a), resonator 3 (Fig. 11b) and the last resonator (Fig. 11c).

From scenario 2 alone, we could conclude that a conventional multiplexing configuration (such as the one in Fig. 6, where the channelizing filters include a SLS in the first resonator) is a suitable topology for obtaining a frequency-selective limiter. However, this conclusion is not supported by the results of scenario 3.

In scenario 3, we see that by locating a SLS in resonator 1, an undesired attenuation effect occurs in the adjacent channel. Placing the SLS in resonator 3 also results in an undesired effect, namely a change on the position of the transmission zeros. This occurs because the cancellation effect produced by the quadruplet section is modified [9]. Finally, from scenario 3, we see that when the multiplexing channels are quite far apart ($f_2 = f_1 + 2.5\mathrm{BW}_1$), a suitable solution is obtained by placing the SLS in the last resonator. In this case a jamming signal in the adjacent channel does not affect the performance at the band of interest. This is because the maximum current in the last resonator follows the same frequency selectivity than the filter transmission response [9].

## V. Conclusion

Although the analysis above corresponds to very specific scenarios, the frequency dependence of the limiting effect in these scenarios enables identification of the optimal location of a SLS in the studied filter topology, and evaluation of the performance of the resulting filter. Further, we can readily extend this study to other types of jamming signals, other filter designs and other multiplexing topologies using the presented approach. We may conclude, therefore, that the equivalent circuit proposed in this work is very useful to design and evaluate limiting systems based on SLS circuit elements.

## References

[1] J. C. Booth, K. Leong, and S. A. Schima, "A superconducting microwave power limiter for high performance receiver protection," in *Proc. IEEE MTT-S Int. Microw. Symp. Dig.*, 2004, vol. 1, pp. 139–142.

[2] J. C. Booth, D. A. Rudman, and R. H. Ono, "A self-attenuating superconducting transmission line for use as a microwave power limiter," *IEEE Trans. Appl. Supercond.*, vol. 13, no. 2, pp. 305–310, Jun. 2003.

[3] E. Rocas *et al.*, "Superconducting multiplexer filter bank for a frequency-selective power limiter," *IEEE Trans. Appl. Supercond.*, vol. 21, no. 3, pp. 542–546, Jun. 2011.

[4] E. Rocas, J. C. Collado, N. Orloff Mateu, and J. C. Booth, "Modeling of self-heating mechanism in the design of superconducting limiters," *IEEE Trans. Appl. Supercond.*, vol. 21, no. 3, pp. 547–550, Jun. 2011.

[5] T. Dahm and D. J. Scalapino, "Theory of intermodulation in superconducting microstrip resonator," *J. Appl. Phys.* vol. 81, no. 4, pp. 2002–2012, Feb. 1997.

[6] W. T. Weeks *et al.*, "Resistive and inductive skin effect in rectangular conductors," *IBM J. Res. Develop.*, vol. 23, pp. 652–660, Nov. 1979.

[7] D. M. Sheen, S. M. Ali, D. E. Oates, R. S. Withers, and J. A. Kong, "Current distribution, resistance, and inductance for superconducting transmission lines," *IEEE Trans. Appl. Supercond.*, vol. 1, no. 3, pp. 108–115, Jun. 1991.

[8] Y.S. Muzychka, J. R. Culham, and M. M. Yovanovich, "Thermal spreading resistance of eccentric heat source on rectangular flux channels," *J. Electron. Packag.*, vol. 125, pp. 178–185, Jun. 2003.

[9] R. J. Cameron, C. M. Kudsia, and R. R. Mansour, *Microwave Filters for Communication Systems. Fundamentals, Design, and Applications*. New York, NY, USA: Wiley, 2007.

[10] C. Collado, A. Hueltes, E. Rocas, J. Mateu, J. C. Booth, and J. M. O'Callaghan, "Absorptive limiter for frequency-selective circuits," *IEEE Microw. Wireless Comp. Lett.*, vol. 24, no. 6, pp. 415–417, Jun. 2014.